Supporting Information

Cerium Pyrazolates Grafted onto Mesoporous Silica SBA-15: Reversible CO_2 Uptake and Catalytic Cycloaddition of Epoxides and Carbon Dioxide

Uwe Bayer, Yucang Liang, and Reiner Anwander*

Institut für Anorganische Chemie, Eberhard Karls Universität Tübingen, Auf der Morgenstelle 18, 72076 Tübingen, Germany

E-Mail: reiner.anwander@uni-tuebingen.de

Table of Contents

PXRD	**S3**
SEM and TEM	**S3**
Decomposition Study	**S4**
NMR Spectra	**S4**
TGA	**S11**
Crystallographic Data	**S12**
References	**S14**

Powder X-Ray Diffraction (PXRD)

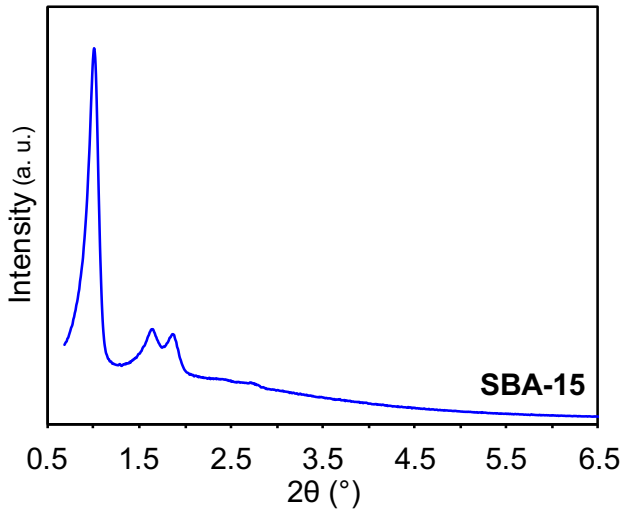

Figure S1. Low-angle PXRD pattern of parent SBA-15.

Scanning/Transmission Electron Microscopy (S/TEM)

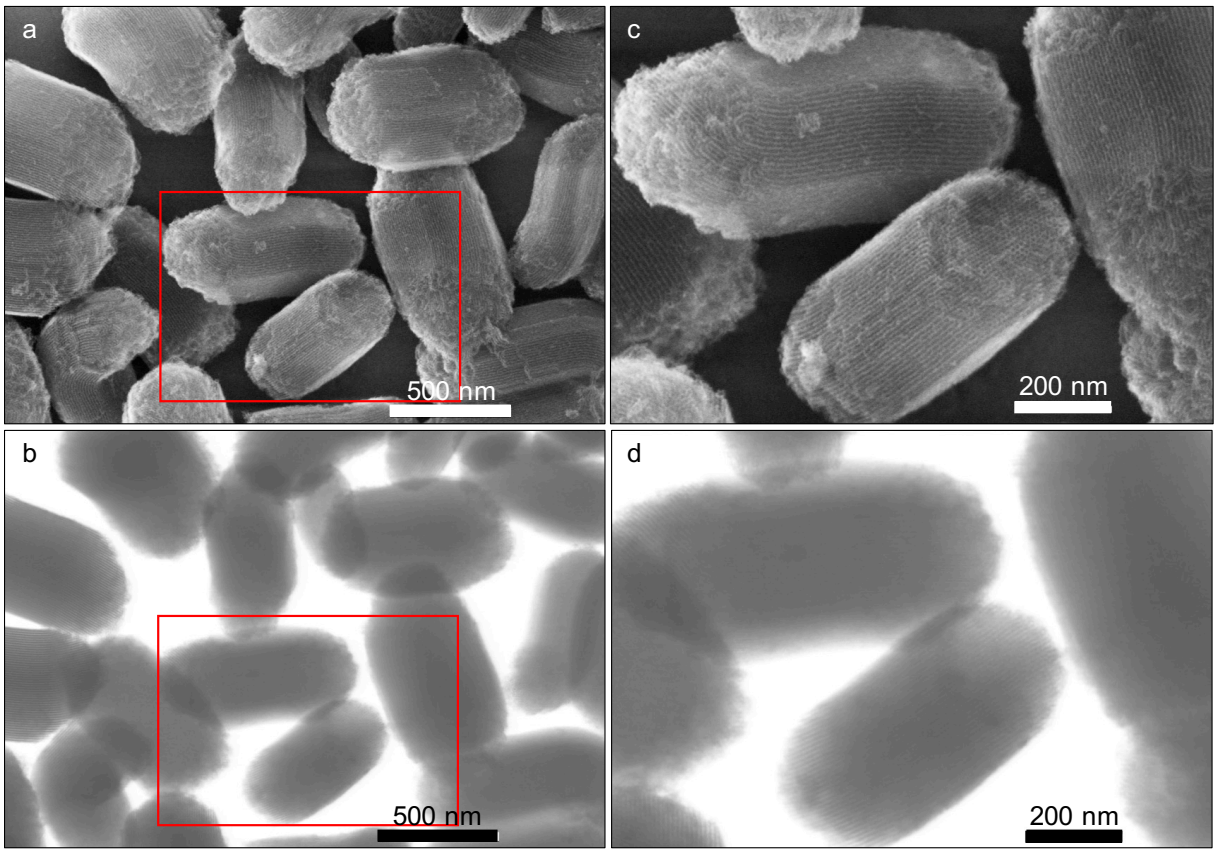

Figure S2. SEM (a,c) and TEM (b,d) images of parent SBA-15; (c) and (d) are magnified views of the red-marked areas in (a) and (b), respectively.

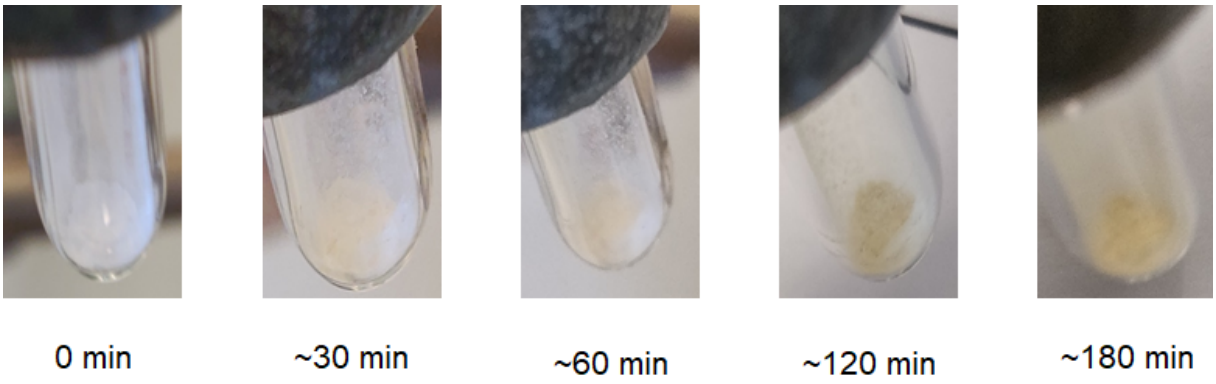

Figure S3. Color change during evacuation of a $[Ce(Me_2pz)_3(thf)]_2$@SBA-15_{500} sample at high vacuum ($p < 9 \cdot 10^{-5}$ mbar) indicating decomposition under reduced pressure.

NMR Spectra (solvent signals are marked with *)

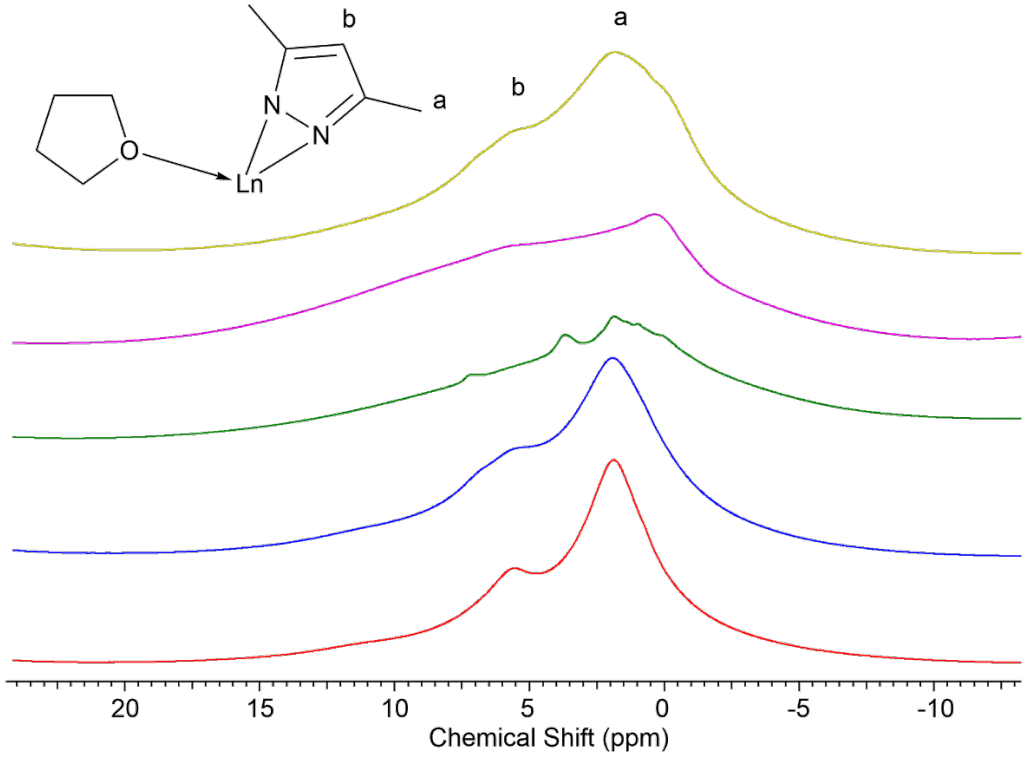

Figure S4. ^{1}H MAS NMR spectra of of $[Ce(Me_2pz)_4]_2$@SBA-15_{500} (**H1**) (red), $Ce(Me_2pz)_4(thf)$@SBA-15_{500} (**H2**) (blue), $Ce_4(Me_2pz)_{12}$@SBA-15_{500} (**H3**) (green), $[Ce(Me_2pz)_3(thf)]_2$@SBA-15_{500} (**H4**) (pink), and $[La(Me_2pz)_3(thf)]_2$@SBA-15_{500} (**H5**) (yellow), from bottom to top.

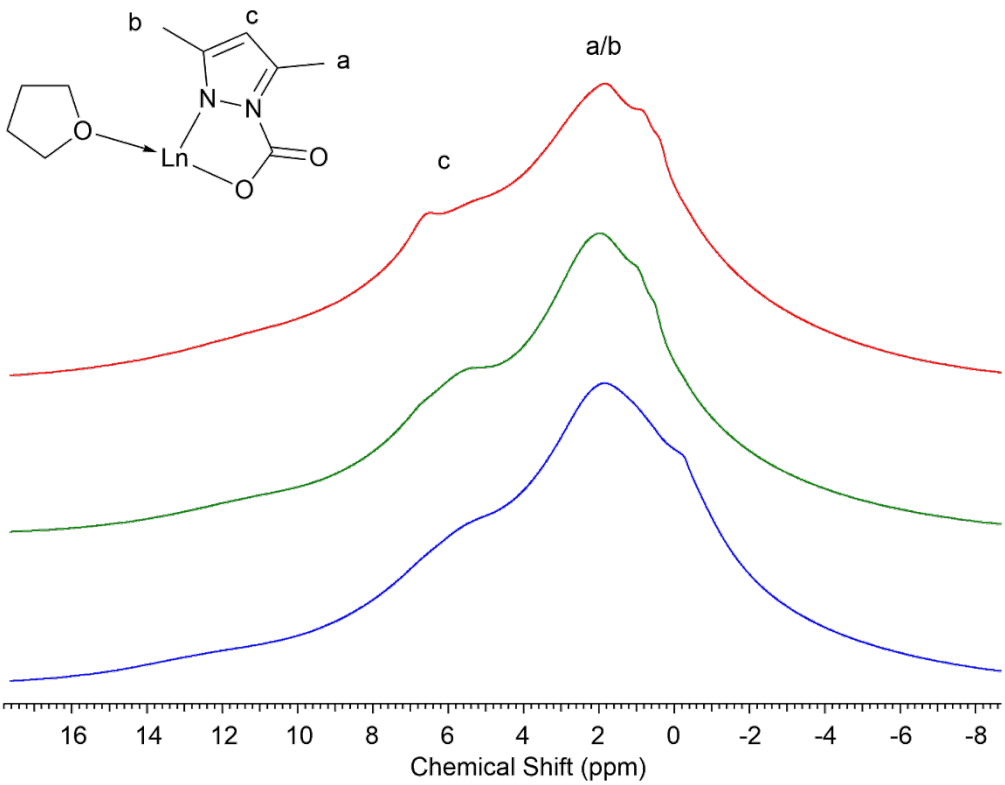

Figure S5. ^{1}H MAS NMR spectra of CO_2@[Ce(Me$_2$pz)$_4$]$_2$@SBA-15$_{500}$ (**H1^{CO2}**) (blue), CO_2@Ce(Me$_2$pz)$_4$(thf)@SBA-15$_{500}$ (**H2^{CO2}**) (green), and CO_2@[La(Me$_2$pz)$_3$(thf)]$_2$@SBA-15$_{500}$ (**H5^{CO2}**) (red) from bottom to top.

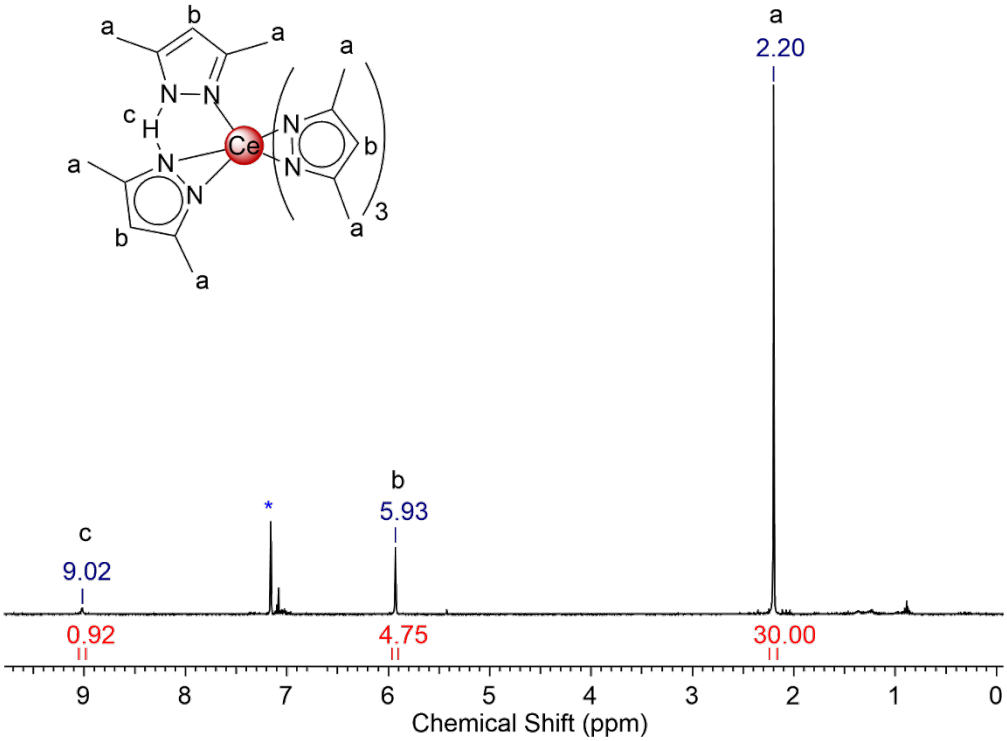

Figure S6. ^{1}H NMR spectrum (C_6D_6, 400.13 MHz, 26 °C) of the non-volatile compounds of the supernatant after grafting of Ce(Me$_2$pz)$_4$(thf) (**H2**). The spectrum shows minor impurities of *n*-hexane and toluene. Solvent signal is marked with an asterisk. Signals are in accordance with literature known Ce(Me$_2$pz)$_4$(Me$_2$pzH).[1]

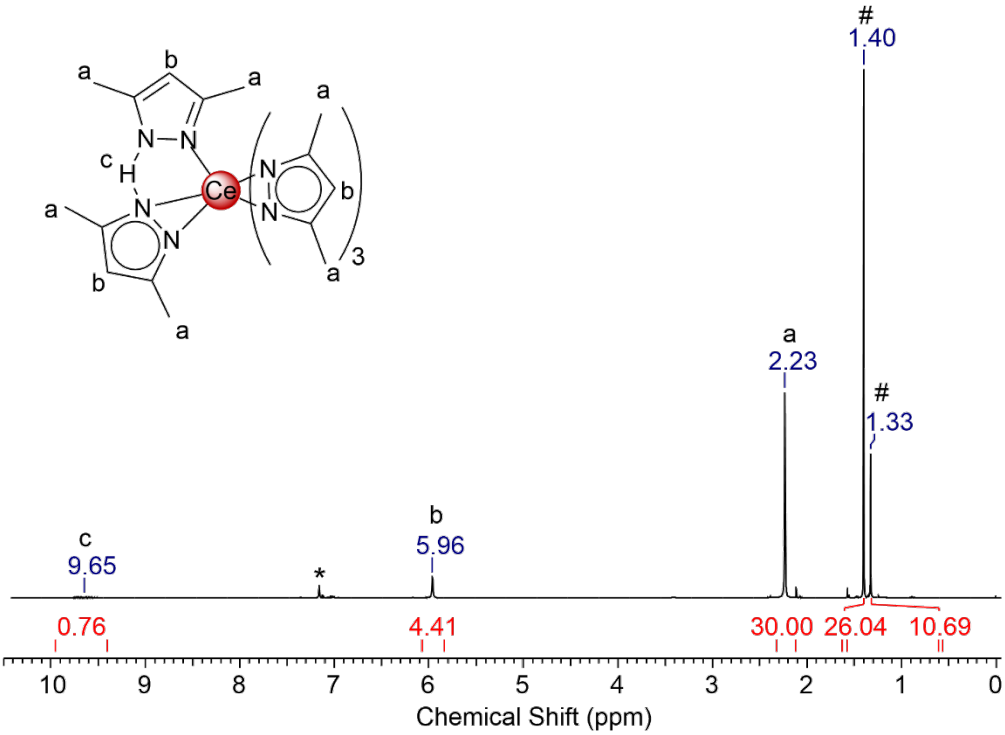

Figure S7. ^{1}H NMR spectrum (C_6D_6, 400.13 MHz, 26 °C) of the reaction mixture of $[Ce(Me_2pz)_4]_2$ and $HOSi(OtBu)_3$ yielding $Ce(Me_2pz)_4(Me_2pzH)$ and an unknown tris-*tert*-butoxysiloxy species (marked with #).

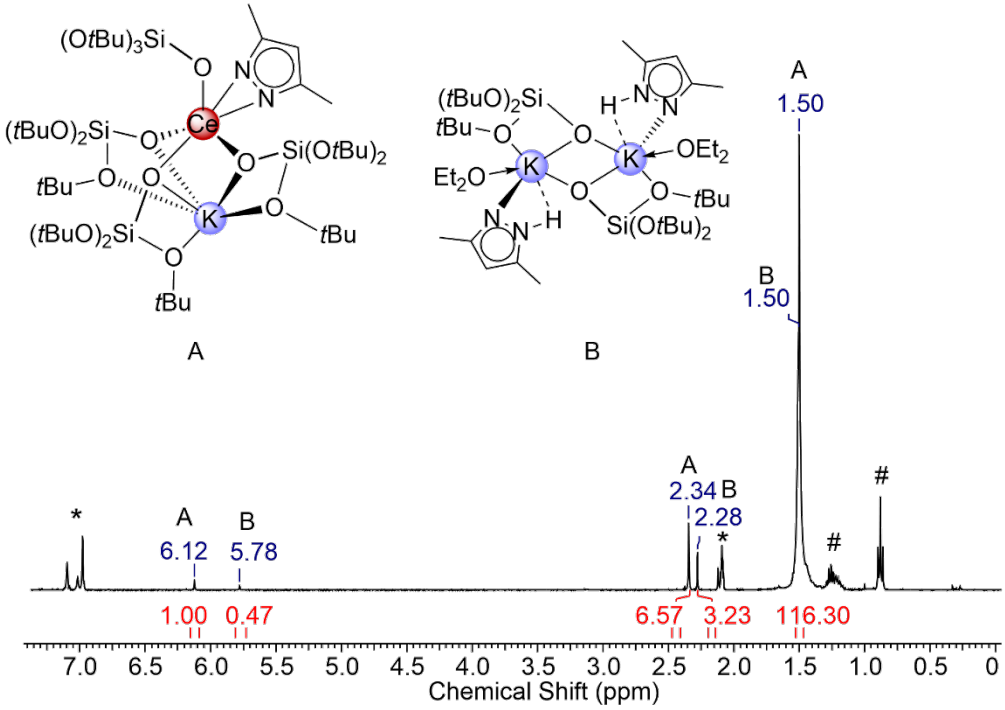

Figure S8. ^{1}H NMR spectrum (toluene-d_8, 400.13 MHz, 26 °C) of a mixture of $KCe[OSi(OBu)_3]_4(Me_2pz)$ (**6**) and $K[OSi(OtBu)_3](Me_2pzH)(Et_2O)$**.** Impurities of *n*-pentane are marked with #.

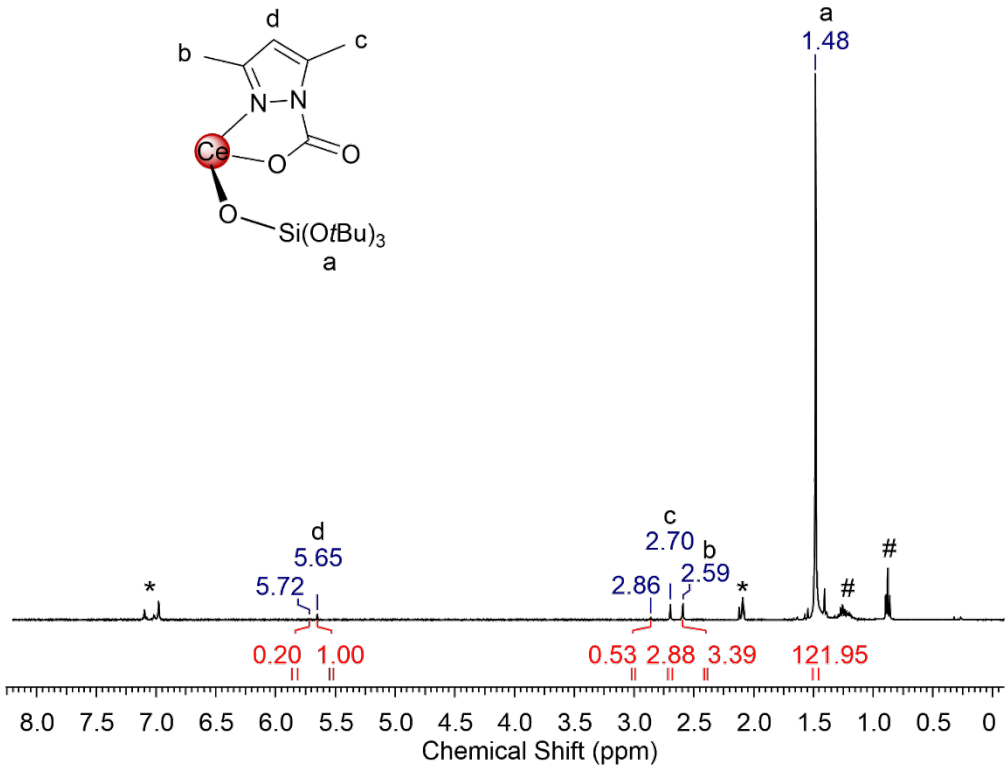

Figure S9. ^{1}H NMR spectrum (toluene-d_8, 400.13 MHz, 26 °C) of the reaction of CO_2 with the mixture KCe[OSi(OBu)$_3$]$_4$(Me$_2$pz) (**6**)/K[OSi(O*t*Bu)$_3$](Me$_2$pzH)(Et$_2$O). Impurities of *n*-pentane are marked with #.

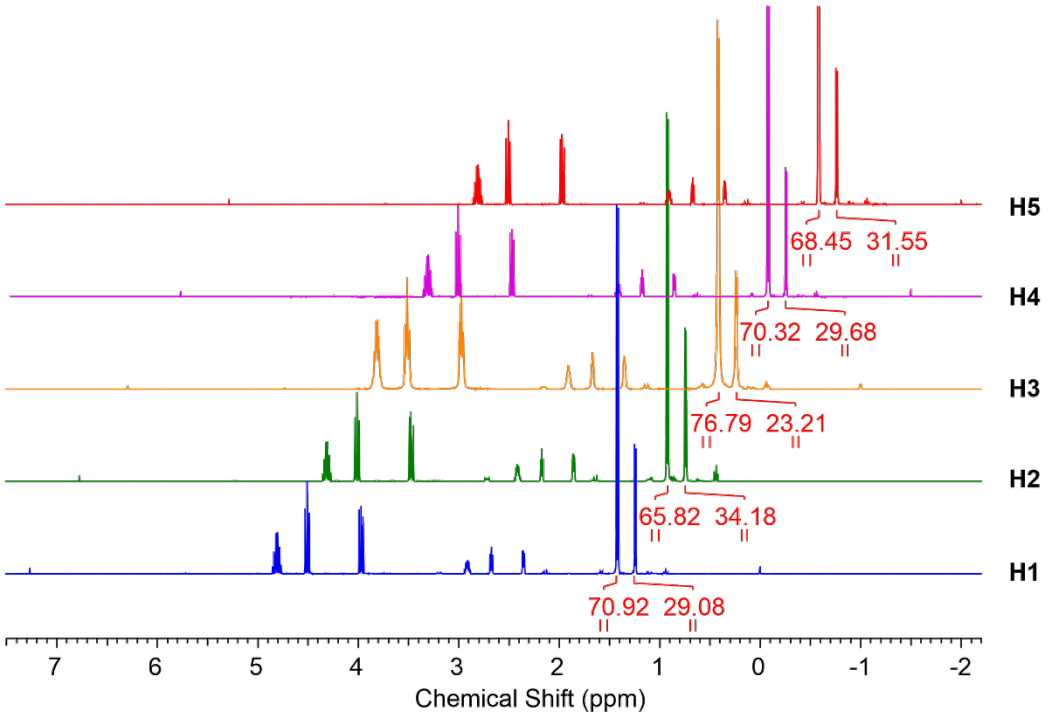

Figure S10. Stacked ^{1}H NMR spectra ($CDCl_3$, 400.13 MHz, 26 °C) of the product mixture of the catalytic formation of propylene carbonate using 0.1 mol% of [Ce(Me$_2$pz)$_4$]$_2$@SBA-15$_{500}$ (**H1**), Ce(Me$_2$pz)$_4$(thf)@SBA-15$_{500}$ (**H2**), Ce$_4$(Me$_2$pz)$_{12}$@SBA-15$_{500}$ (**H3**), [Ce(Me$_2$pz)$_3$(thf)]$_2$@SBA-15$_{500}$ (**H4**) , or [La(Me$_2$pz)$_3$(thf)]$_2$@SBA-15$_{500}$ (**H5**) and TBAB as a catalyst system. The conversion was determined by the integral ratio of the methyl protons in propylene oxide and propylene carbonate.

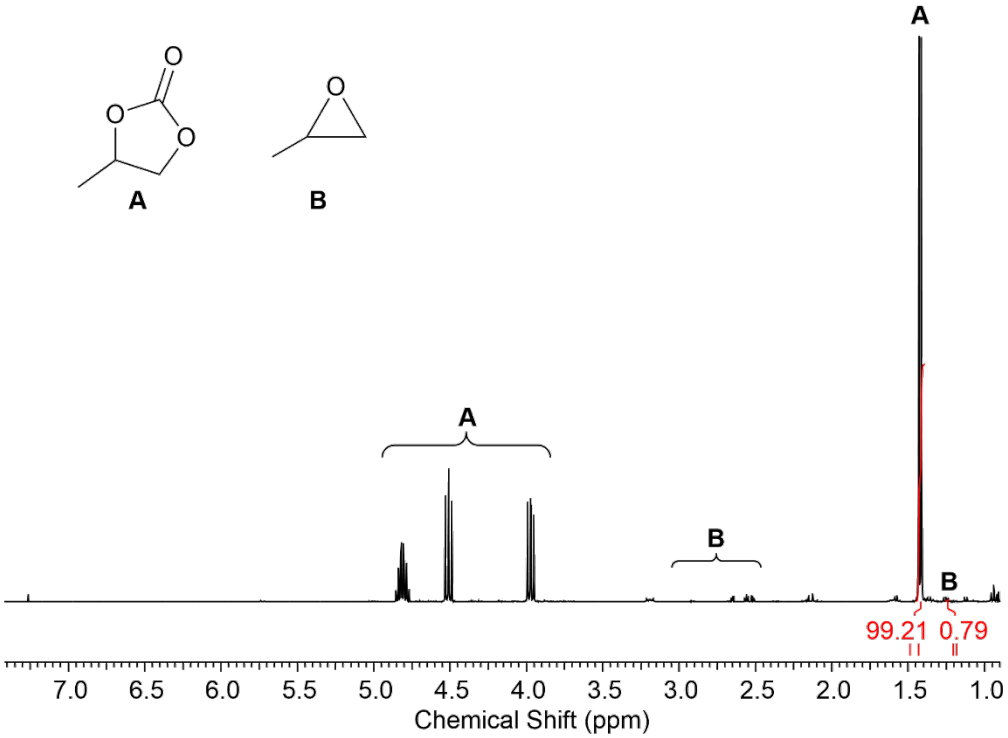

Figure S11. ^{1}H NMR (26 °C, 400.13 MHz, chloroform-*d*) of the product mixture of the catalytic formation of propylene carbonate using 0.5 mol% of $[Ce(Me_2pz)_4]_2$@SBA-15_{500} (**H1**) and TBAB as a catalyst system. The conversion was determined by the integral ratio of the methyl protons in propylene oxide and propylene carbonate.

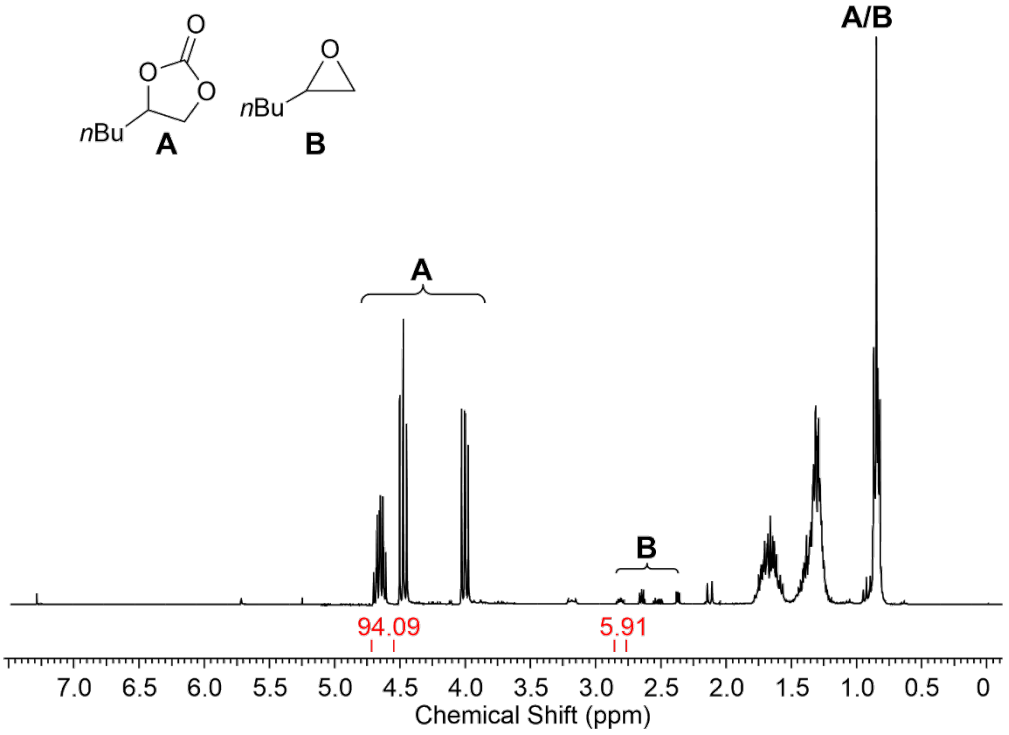

Figure S12. ^{1}H NMR (26 °C, 400.13 MHz, chloroform-*d*) of the product mixture of the catalytic formation of 1,2-*n*-hexylene carbonate using 0.5 mol% of $[Ce(Me_2pz)_4]_2$@SBA-15_{500} (**H1**) and TBAB as a catalyst system. The conversion was determined by the integral ratio of the protons in *α*-position in 1,2-*n*-hexylene oxide and 1,2-*n*-hexylene carbonate.

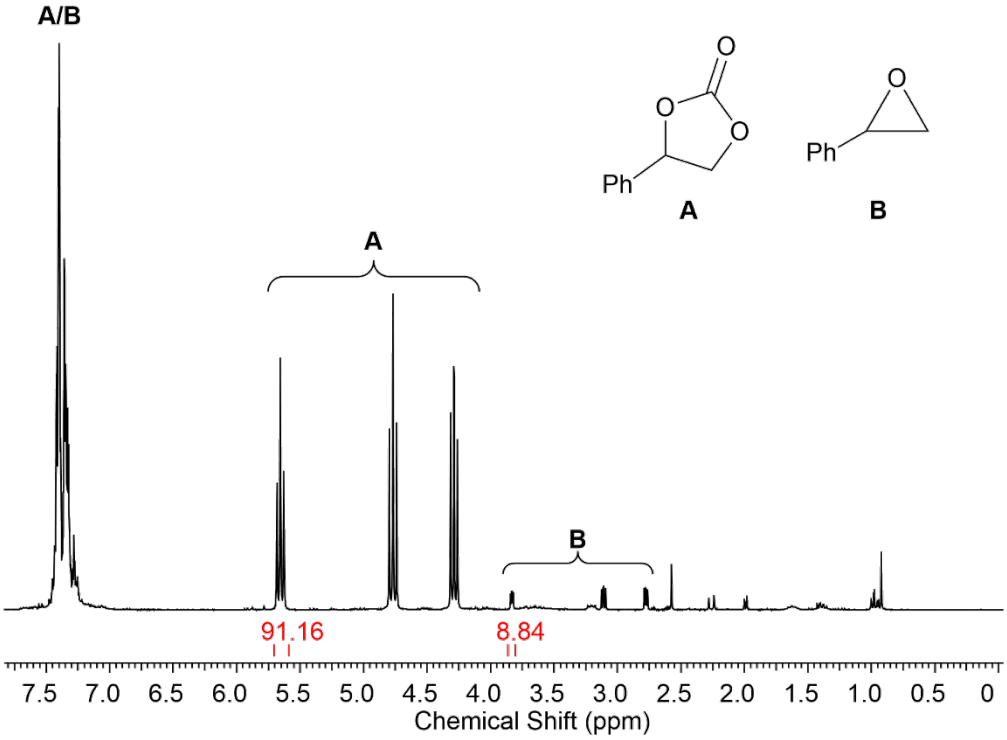

Figure S13. ^{1}H NMR (26 °C, 400.13 MHz, chloroform-*d*) of the product mixture of the catalytic formation of styrene carbonate using 0.5 mol% of $[Ce(Me_2pz)_4]_2$@SBA-15_{500} (**H1**) and TBAB as a catalyst system. The conversion was determined by the integral ratio of the protons in *α*-position in styrene oxide and styrene carbonate.

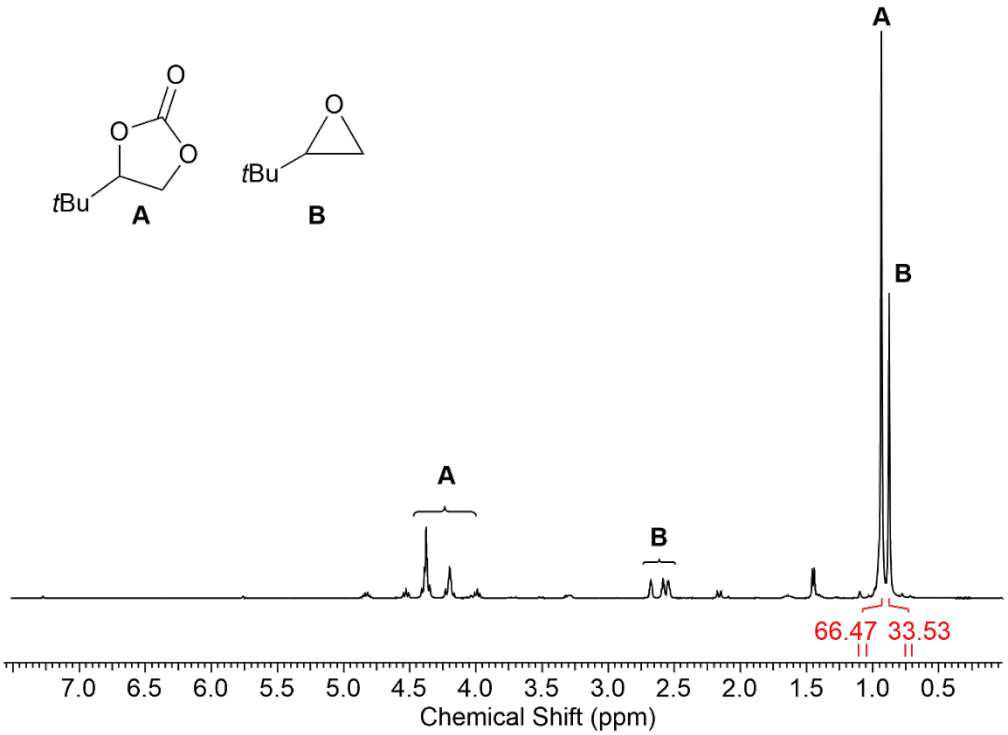

Figure S14. ^{1}H NMR (26 °C, 400.13 MHz, chloroform-*d*) of the product mixture of the catalytic formation of 3,3-dimethyl-1,2-butylene carbonate using 0.5 mol% of $[Ce(Me_2pz)_4]_2$@SBA-15_{500} (**H1**) and TBAB as a catalyst system. The conversion was determined by the integral ratio of the *tert*-butyl protons in 3,3-dimethyl-1,2-butene oxide and 3,3-dimethyl-1,2-butylene carbonate.

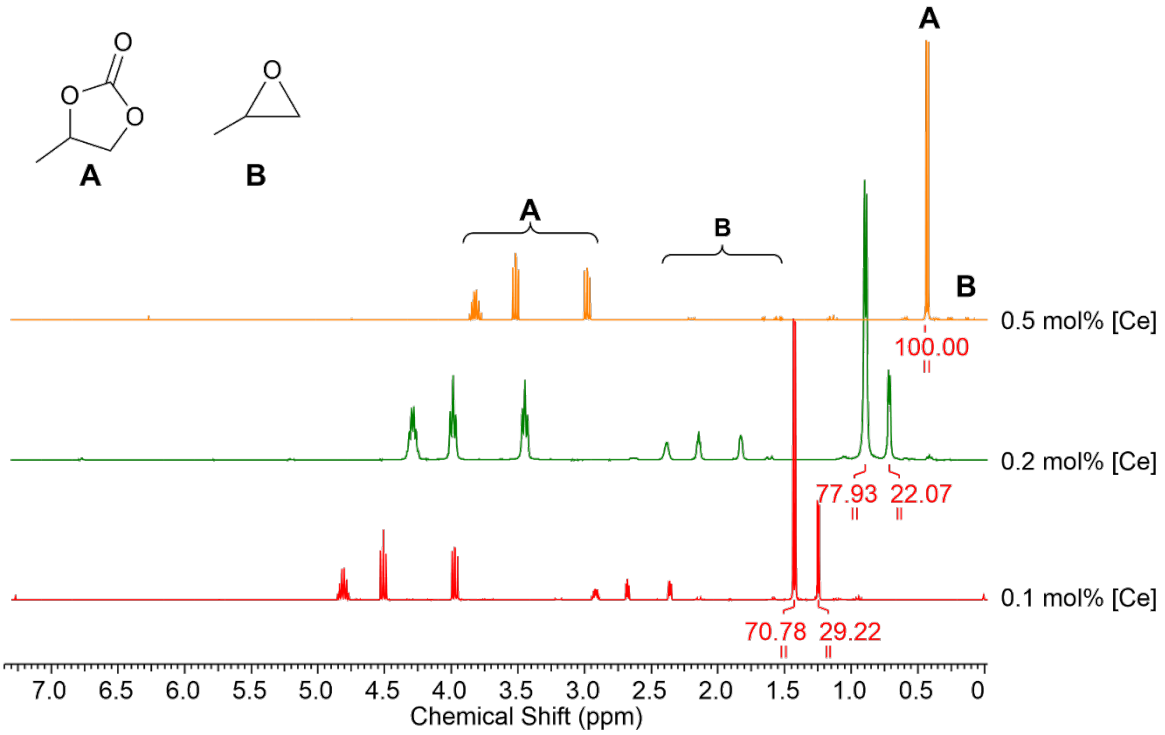

Figure S15. Stacked ^{1}H NMR spectra ($CDCl_3$, 400.13 MHz, 26 °C) of the product mixture of the catalytic formation of propylene carbonate using different amounts of $[Ce(Me_2pz)_4]_2$@SBA-15_{500} (**H1**) and TBAB as a catalyst system. The conversion was determined by the integral ratio of the methyl protons in propylene oxide and propylene carbonate.

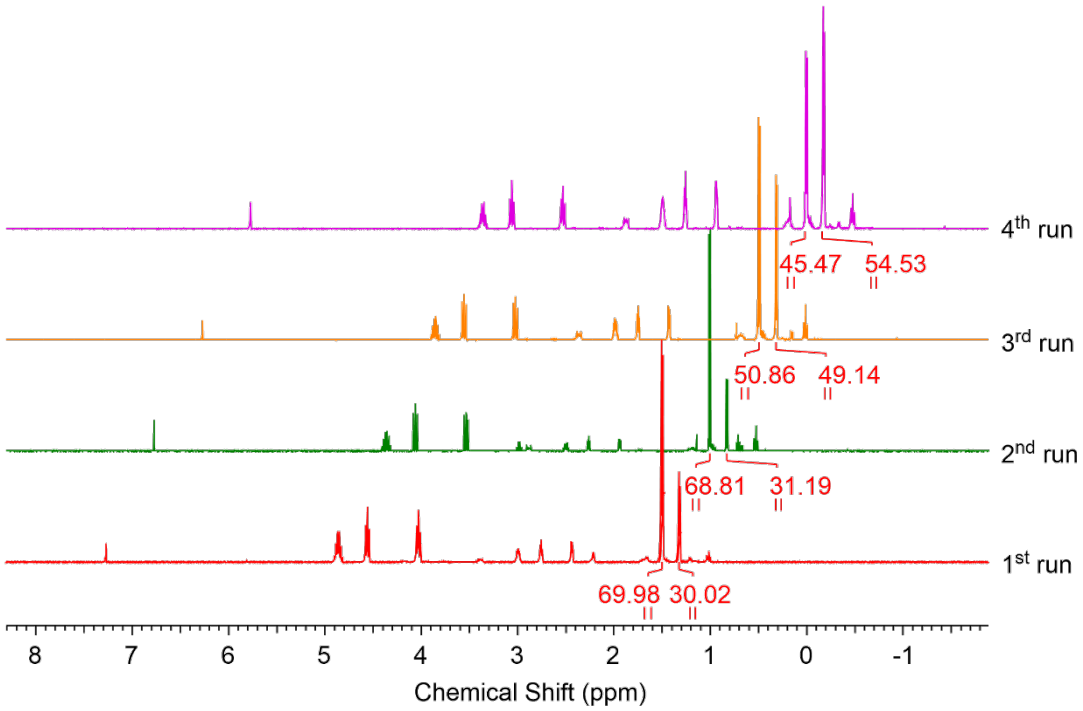

Figure S16. Stacked ^{1}H NMR spectra ($CDCl_3$, 400.13 MHz, 26 °C) of the product mixture of the catalytic formation of propylene carbonate using 0.5 mol% of $Ce(Me_2pz)_4(thf)$@SBA-15_{500} (**H2**) and TBAB as a catalyst system. The conversion was determined by the integral ratio of the methyl protons in propylene oxide and propylene carbonate.

TGA

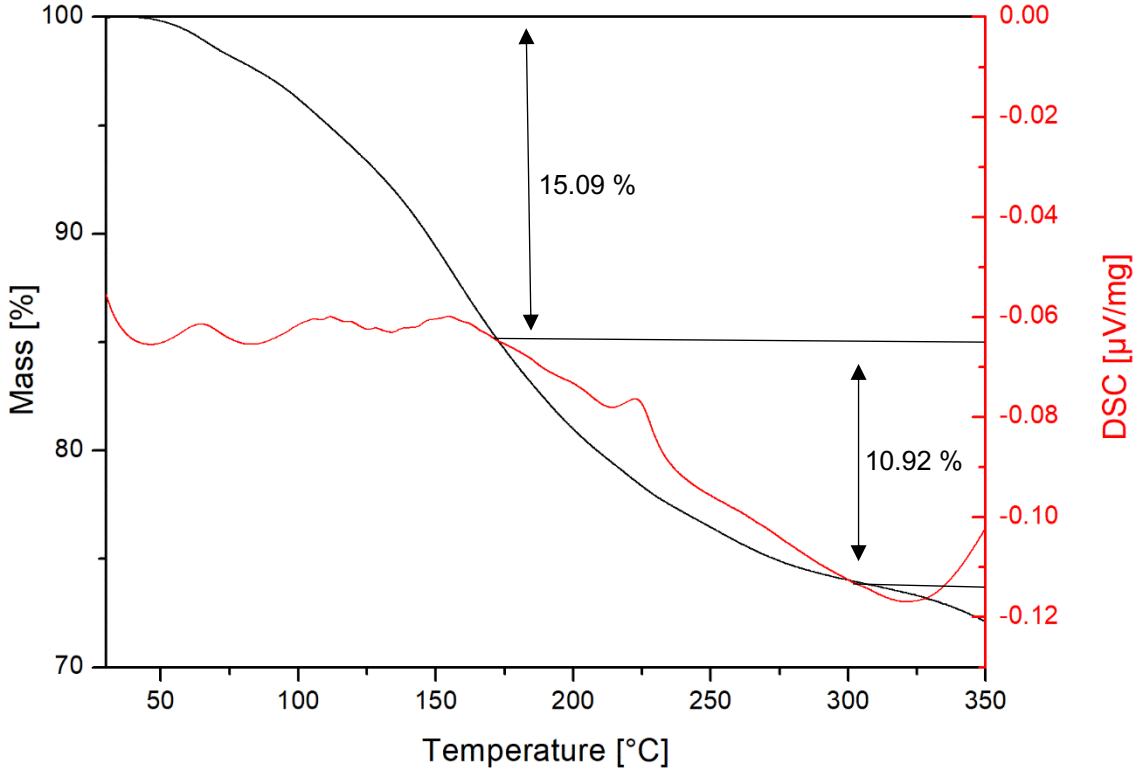

Figure S17. Thermogravimetric analysis (red) and differential scanning calorimetry (red) of CO_2@[La(Me_2pz)$_3$(thf)]$_2$@SBA-15$_{500}$ (**H5^{CO2}**).

Crystallographic Data

Crystals for X-ray crystallography were grown using saturated solutions of mixtures of *n*-pentane / Et_2O (**6** and K[OSi(O*t*Bu)$_3$](Me$_2$pzH)(Et_2O)). Suitable crystals for X-ray analysis were handpicked in a glovebox, coated with Parabar 10312 and stored on microscope slides. Data collection was done on a *Bruker* APEX II Duo diffractometer by using QUAZAR optics and Mo K_α (λ = 0.71073 Å). The data collection strategy was determined using COSMO[2] employing ω scans. Raw data were processed by APEX and SAINT,[3,4] corrections for absorption effects were applied using SADABS.[5] The structures were solved by direct methods and refined against all data by full-matrix least-squares methods on F^2 using SHELXTL and SHELXLE.[6,7] All non-hydrogen atoms were refined anisotropically. Plots were generated by using CCDC Mercury 3.19.1.[8] Further details regarding the refinement and crystallographic data are listed in Table S1 and in the CIF files.

Table S1. Crystallographic data for compounds **6** and K[OSi(O*t*Bu)$_3$](Me$_2$pzH)(Et$_2$O)

	6	K[OSi(O*t*Bu)$_3$](Me$_2$pzH)(Et$_2$O)
CCDC	2023873	2023872
formula	$C_{53}H_{115}CeKN_2O_{16}Si_4$	$C_{42}H_{90}K_2N_4O_{10}Si_2$
M [g·mol^{-1}]	1328.04	945.55
λ [Å]	0.71073	0.71073
color	orange-yellow	colorless
crystal dimensions [mm]	0.379 × 0.254 × 0.114	0.512 × 0.299 × 0.292
crystal system	monoclinic	triclinic
space group	$P2_1/n$	$P\bar{1}$
a [Å]	16.7561(7)	11.5002(5)
b [Å]	19.8676(9)	12.0299(5)
c [Å]	21.7572(9)	12.7116(5)
α [°]	90	115.5620(10)
β [°]	98.9390(10)	96.0850(10)
γ [°]	90	113.5980(10)
V [Å^3]	7155.1(5)	1368.67(10)
Z	4	1
F(000)	2832	516
T [K]	100(2)	100(2)
ρ_{calcd} [g·cm^{-3}]	1.233	1.147
μ[mm^{-1}]	0.818	0.268
Data / restraints / parameters	20044 / 18 / 732	9093 / 0 / 288
Goodness of fit	1.038	1.042
R_1 (I > 2σ (I))[a]	0.0281	0.0289
$_\omega R_2$ (all data)[b]	0.0719	0.0808

[a] $R_1 = \Sigma(||F0|-|Fc||)/\Sigma|F0|, F0> 4s(F0)$. $_\omega R_2 = \{\Sigma[w(F02-Fc2)2/\Sigma[w(F02)^2]\}^{1/2}$

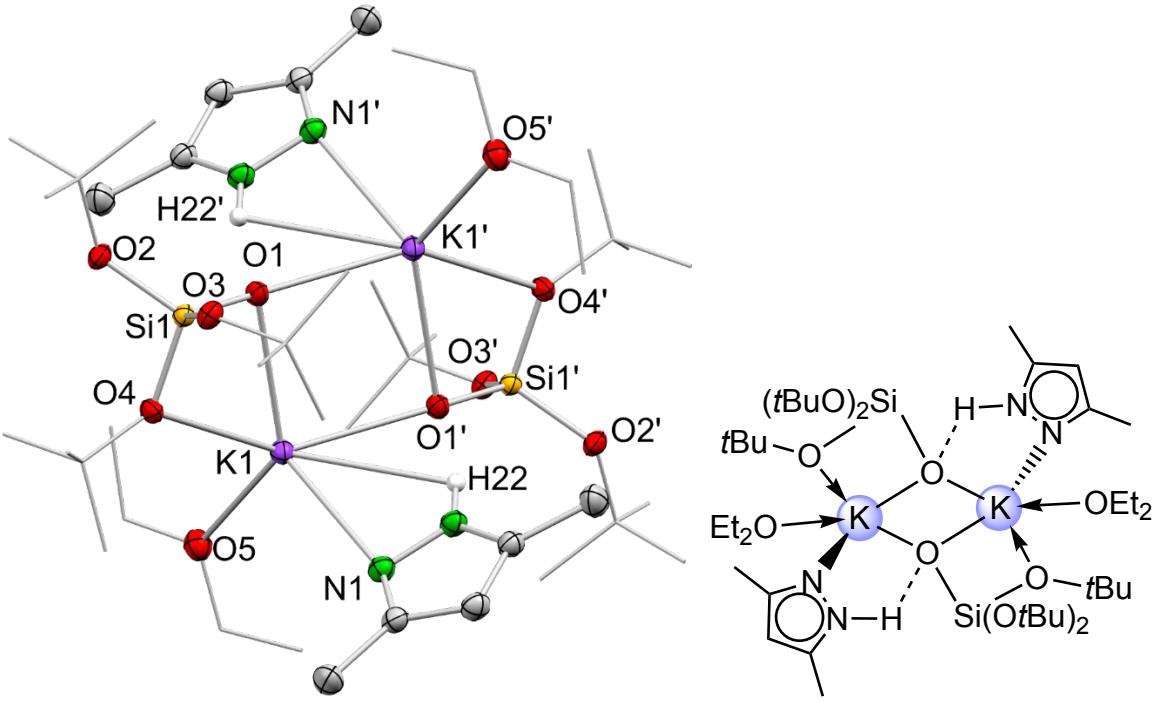

Figure S18. Crystal structure and structural representation of K[OSi(O*t*Bu)$_3$](Me$_2$pzH)(Et$_2$O). Ellipsoids are shown at the 50% probability level. Hydrogen atoms are omitted for clarity. Selected bond lengths [Å]: K1−O1 2.7686(6), K1−O4 2.7338(6), K1−O1' 2.6308(6), K1−N1 2.8604(7), K1−H22 2.902(14).

References

(1) Werner, D.; Bayer, U.; Schädle, D.; Anwander, R. Emergence of a New [NNN] Pincer Ligand via Si-H-Bond Activation and β-Hydride Abstraction at Tetravalent Cerium. *Chem. - Eur. J.* **2020**, *26*, 12194–12205.

(2) *COSMO, v. 1.61*; Bruker AXS Inc.: Madiso, Wi, **2012**.

(3) *APEX 3, v. 2016.5-0*; Bruker AXS Inc.: Madison, Wi, **2012**.

(4) *Saint, v. 8.34A*; Bruker AXS Inc.: Madison, Wi, **2012**.

(5) Krause, L.; Herbst-Irmer, R.; Sheldrick, G. M.; Stalke, D. Comparison of Silver and Molybdenum Microfocus X-Ray Sources for Single-Crystal Structure Determination. *J. Appl. Crystallogr.* **2015**, *48*, 3–10.

(6) Sheldrick, G. M. *SHELXT* – Integrated Space-Group and Crystal-Structure Determination. *Acta Crystallogr. Sect. Found. Adv.* **2015**, *71*, 3–8.

(7) Hübschle, C. B.; Sheldrick, G. M.; Dittrich, B. *ShelXle* : A Qt Graphical User Interface for *SHELXL*. *J. Appl. Crystallogr.* **2011**, *44*, 1281–1284.

(8) Macrae, C. F.; Bruno, I. J.; Chisholm, J. A.; Edgington, P. R.; McCabe, P.; Pidcock, E.; Rodriguez-Monge, L.; Taylor, R.; van de Streek, J.; Wood, P. A. *Mercury CSD 2.0* – New Features for the Visualization and Investigation of Crystal Structures. *J. Appl. Crystallogr.* **2008**, *41*, 466–470.